

Fault Diagnosis and Fault-Tolerant Control of DC-link Voltage Sensor for Two-stage Three-Phase Grid-Connected PV Inverters

Gwang-Seob Kim*, Kyo-Beum Lee[†], Dong-Choon Lee**
 and Jang-Mok Kim***

Abstract – This paper proposes a method for fault diagnosis and fault-tolerant control of DC-link voltage sensor for two-stage three-phase grid-connected PV inverters. Generally, the front-end DC-DC boost converter tracks the maximum power point (MPP) of PV array and the rear-end DC-AC inverter is used to generate a sinusoidal output current and keep the DC-link voltage constant. In this system, a sensor is essential for power conversion. A sensor fault is detected when there is an error between the sensed and estimated values, which are obtained from a DC-link voltage sensorless algorithm. Fault-tolerant control is achieved by using the estimated values. A deadbeat current controller is used to meet the dynamic characteristic of the proposed algorithm. The proposed algorithm is validated by simulation and experiment results.

Keywords: Fault diagnosis, Fault-tolerant control, Grid-connected inverter, Sensorless control, PV inverters, Deadbeat control

1. Introduction

The generation of renewable power (e.g., wind and solar power) for supplementing the generation of conventional power has drawn considerable attentions [1]. A photovoltaic (PV) panel is the one of the most promising devices for the generation of renewable energy since it can convert solar energy to electric energy directly [2-4].

A grid-connected PV generation system is generally classified as single-stage or two-stage configuration according to the number of processing stage, as illustrated in Fig. 1. The single-stage topology (Fig. 1(a)) compose one inverter to carry out both maximum power point tracking (MPPT) and pulse width modulation (PWM), which is regarded as the most reliable and cost effective structure. However, because of the limitation of the minimum DC-link voltage for the operation of grid-connected inverter and the rated voltage of switch, there are many restrictions on the MPPT operation. To overcome the limitation, the two-stage configuration is used. The two-stage topology (Fig. 1(b)) consisting of DC-DC boost converter and DC-AC inverter can enlarge the MPPT operation range for PV grid-connected system. Using a DC-DC boost converter in front, the efficiency of whole inverter system would decrease since more passive and

active components (IGBT, capacitor, inductor, diode) are involved in the energy processing when compared to the single-stage topology but when considering the improved MPPT efficiency and wide operation range the two-stage solution is superior to the single-stage inverter [5, 6].

The MPPT algorithms focus largely on the perturbation and observation (P&O) method and the incremental conductance (IC) methods. They usually require the PV voltage and current values measured by voltage and current

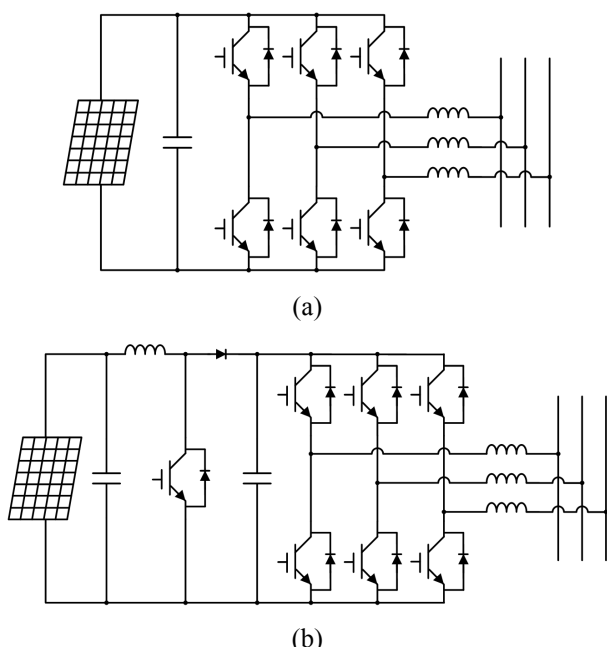


Fig. 1. The topology of (a) single-stage and (b) two-stage three-phase grid-connected PV systems

* Corresponding Author: Department of Electrical and Computer Engineering, Ajou University, Suwon, Korea. (kyl@ajou.ac.kr)

† Department of Electrical and Computer Engineering, Ajou University, Suwon, Korea. (bhj8@ajou.ac.kr)

** Department of Electrical Engineering, Yeungnam University, Korea. (dclee@yu.ac.kr)

*** Department of Electrical Engineering, Pusan National University, Korea. (jmok@pusan.ac.kr)

Received: June 4, 2012; Accepted: December 14, 2012

sensors for calculating the present power and for tracking the maximum power point. In the rear-end inverter, a voltage sensor across a DC-link capacitor is essential for DC-link voltage control to measure the DC-link voltage value so that the PV inverter can operate stably. As mentioned previously, since sensors are essential components for the construction of an inverter system, fault diagnosis of the sensors and fault-tolerant control are necessary [7-9].

This paper proposes a fault diagnosis and fault-tolerant control of a DC-link voltage sensor for two-stage three-phase grid-connected PV inverters. If the DC-link voltage sensor breaks down, the fault is determined by comparing the error rate of sensed and estimated voltage. The estimated voltage is obtained by using the DC-link voltage sensorless method. After detecting the fault, the PV inverter is implemented by the estimated voltage. This fault-tolerant control method can be used to keep the system stable during system operation without sacrificing either output performance or MPPT accuracy. For fault diagnosis and fault-tolerant control, the current controller must have very fast dynamic characteristics for operating safely. The deadbeat current controller provides a fast transient response and accurate current tracking [10, 11]. The algorithm proposed in this paper shows the MPPT control to be operating smoothly under fault-tolerant control. A PSIM simulation and an experiment using a PV power conditioning system (PCS) are performed to verify the effectiveness of the proposed algorithm.

2. Description of the grid-connected PV system

The configuration of the grid-connected PV system is shown in Fig. 2. The output of the PV panel depends on environmental conditions such as the temperature, solar irradiance, angle-of-incidence, solar spectrum (air mass), and the types of PV cells used in the panel. The front-end

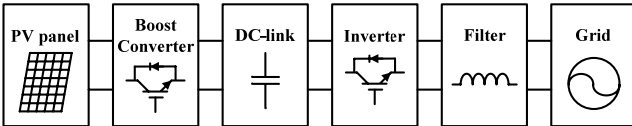


Fig. 2. The configuration of the grid-connected PV system

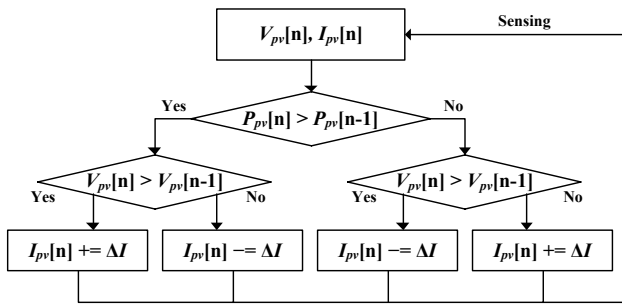


Fig. 3. The progress of P&O algorithm

DC-DC boost converter tracks the maximum power point (MPP) of the PV panel by measuring the input current and voltage. The voltage across the DC-link capacitor can be kept at a constant value by controlling the power flow. The rear-end DC-AC inverter is used to transform DC power into AC power with high waveform quality. The output current from the inverter enters the grid after passing through the filters.

2.1 MPPT control using a boost converter

MPPT control is important to extract the maximum power under various external conditions [12]. The P&O method is applied in many practical PV systems because it makes calculations easy.

In the P&O algorithm, the PV output power is obtained by multiplying the PV voltage with the PV current. First, the PV voltage & PV current are set at their initial values. Then, perturbations are induced to observe and compare the values of PV output power captured before and after the perturbation. Finally, the PV output power tracks the maximum power point (MPP) of the PV panel by using a multi-stepped technique. The progress of the P&O algorithm is shown in Fig. 3 [9].

2.2 Grid-connected inverter

The configuration of the grid-connected inverter is shown in Fig. 4. The superscript “^” refers to the estimated variables and quantities, and the superscript “*” denotes

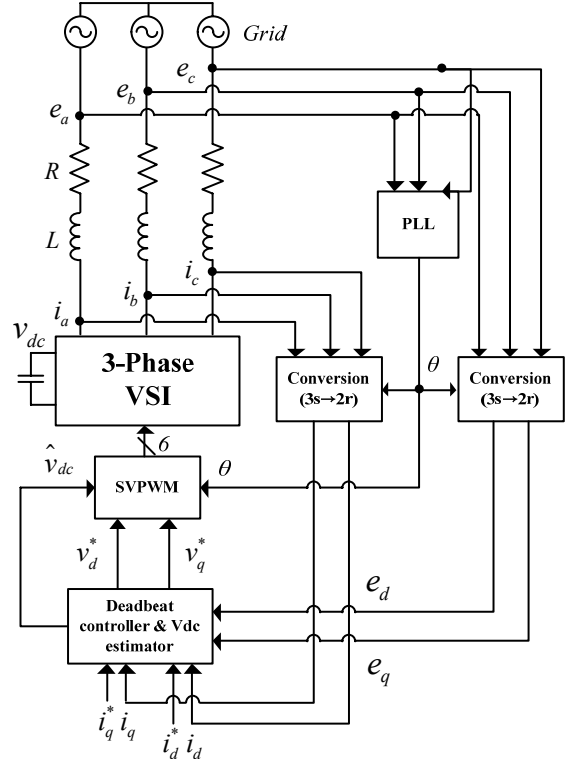


Fig. 4. The configuration of grid-connected inverter

the reference variables and quantities. The current (i_a , i_b , i_c) and voltage (e_a , e_b , e_c) variables transform from the three-phase stationary coordinate system to the two-phase rotating coordinate system. The deadbeat controller uses the q-axis current to influence the output current into following its reference and the DC-link voltage estimator assumes the real DC-link voltage. The grid angle (θ) is obtained by inverse coordinate transformation by using a phase locked loop (PLL). Knowledge of the values of \hat{v}_{dc} , v_d^* , and v_q^* is necessary for the implementation of space vector pulse width modulation (SVPWM). The fault diagnosis and fault-tolerant control of the DC-link voltage sensor are performed by using the estimated DC-link voltage.

2.3 Deadbeat current controller

In Fig. 4, the voltage equation is

$$\begin{cases} v_d^*(t) = Ri_d(t) + L \frac{di_d(t)}{dt} - \omega L i_q(t) + e_d(t) \\ v_q^*(t) = Ri_q(t) + L \frac{di_q(t)}{dt} + \omega L i_d(t) + e_q(t) \end{cases} \quad (1)$$

For discrete conversion, current is replaced with the following expressions:

$$\begin{cases} \frac{di_d(t)}{dt} \approx \frac{i_d(n+1) - i_d(n)}{T_s} \\ \frac{di_q(t)}{dt} \approx \frac{i_q(n+1) - i_q(n)}{T_s} \end{cases} \quad (2)$$

$$\begin{cases} i_d(t) \approx \frac{i_d(n+1) + i_d(n)}{2} \\ i_q(t) \approx \frac{i_q(n+1) + i_q(n)}{2} \end{cases} \quad (3)$$

The next state value of current for deadbeat control can be written as shown below:

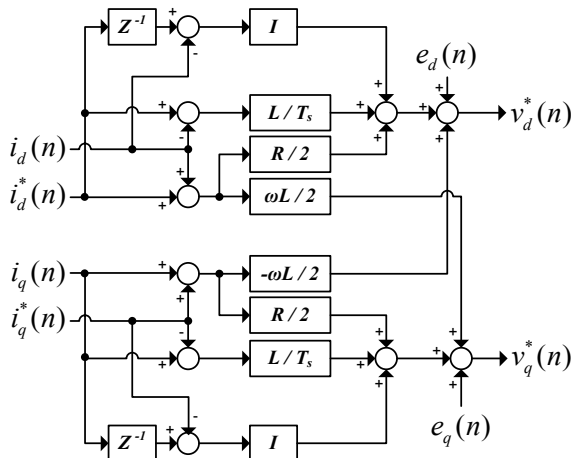


Fig. 5. The block diagram of the deadbeat current controller

$$\begin{cases} i_d(n+1) \approx i_d^*(n) \\ i_q(n+1) \approx i_q^*(n) \end{cases} \quad (4)$$

Through experiments, we found that $i_{d,q}$ cannot follow its reference very well. To guarantee that $i_{d,q}$ follows $i_{d,q}^*$ accurately, an integral (I) controller is added to the control system, as given by in (5) [13].

$$\begin{cases} F(i_d(n)) = F(i_d(n-1)) + K_I T_s (i_d^*(n-1) - i_d(n)) \\ F(i_q(n)) = F(i_q(n-1)) + K_I T_s (i_q^*(n-1) - i_q(n)) \end{cases} \quad (5)$$

The voltage equation can be written as shown below:

$$\begin{cases} v_d^*(n) = R \frac{i_d^*(n) + i_d(n)}{2} + L \frac{i_d^*(n) - i_d(n)}{T_s} \\ \quad - \omega L \frac{i_q^*(n) + i_q(n)}{2} + e_d(n) + F(i_d(n)) \\ v_q^*(n) = R \frac{i_q^*(n) + i_q(n)}{2} + L \frac{i_q^*(n) - i_q(n)}{T_s} \\ \quad + \omega L \frac{i_d^*(n) + i_d(n)}{2} + e_q(n) + F(i_q(n)) \end{cases} \quad (6)$$

Fig. 5 shows the block diagram of the deadbeat current controller.

3. Fault Diagnosis and Fault-tolerant Control of the DC-link Voltage Sensor

3.1 Fault diagnosis

The internal structure of the voltage sensor is shown in Fig. 6. The input current is generated by the input voltage and external resistance that create the primary magnetic flux. The magnetic flux is linked to a magnetic circuit. The Hall device in the air gapped magnetic core provides a voltage that is proportional to the magnetic flux. The voltage is increased by a current amplifier and the increased voltage is used to generate the output current. The output current multiplies as secondary winding turns.

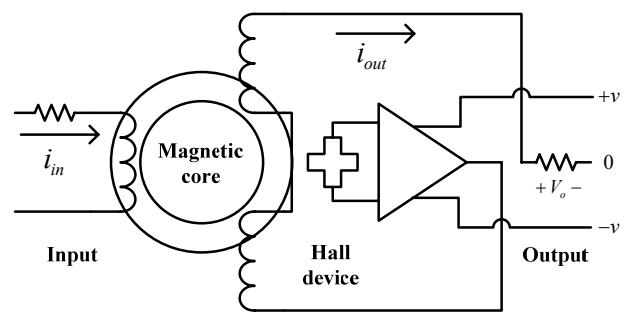


Fig. 6. The internal structure of the voltage sensor

The current generates the primary magnetic flux. Therefore, the output current is exactly proportional to the input current at any instant. The value of the output voltage is obtained from the values of the output current and the measured resistance.

In the voltage sensor structure, the voltage across the DC-link capacitor can be measured since the input and output voltages have a specific relation. The major reasons for an electric sensor fault are gain, offset, saturation, and open circuit faults. This paper focuses mainly on gain and offset faults.

When a fault occurs, the fault is detected by making a comparison between the measured and estimated voltages. To determine the existence of a fault, the error rate is calculated by the following formula:

$$v_{err} = \frac{v_{dc} - \hat{v}_{dc}}{\hat{v}_{dc}} \quad (7)$$

The error rate obtained is compared with the error range (K) to detect a fault, as shown in Eq. (8). As a result of experiments, the error range set to 5% to ensure safe operation during the DC-link voltage sensor fault.

$$|v_{err}| \geq K \quad (8)$$

3.2 Fault-tolerant control

A conventional DC-link voltage and current PI controller is shown in Fig. 7. In the inverter, the d-axis component represents the reactive component and the q-axis component represents the active component. By considering only the active component, the reference of q-axis current is the output of the DC-link voltage PI controller.

To apply the DC-link voltage sensorless control method, the estimated DC-link voltage ($\hat{v}_{dc}(t)$) and the reference of q-axis current ($i_q^*(t)$) are added to (1), as shown in Eq. (9) [14].

$$\frac{\hat{v}_{dc}(t)}{v_{dc}(t)} v_q^*(t) = R i_q^*(t) + L \frac{di_q^*(t)}{dt} + \omega L i_d(t) + e_q(t) \quad (9)$$

Under the deadbeat controller well works, if the estimated DC-link voltage and the measured DC-link voltage are same, the Eq. (9) is equal to the Eq. (1).

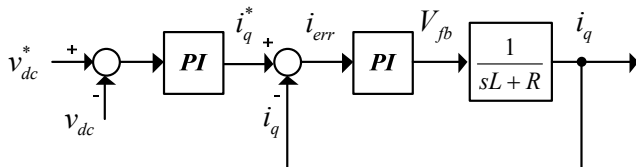


Fig. 7. The conventional DC-link voltage and current controller

The Eq. (9) is a non-linear function. If the estimated DC-link voltage is very close to the measured DC-link voltage in steady state, (9) is linearized, and (1) is used to simplify (9)

$$\hat{v}_{dc}(t) = v_{dc}(t) + \frac{v_{dc}(t)}{v_q^*(t)} R (i_q^*(t) - i_q(t)) + L \frac{d}{dt} (i_q^*(t) - i_q(t)) \quad (10)$$

If the difference between the reference of q-axis currents and the measured q-axis currents is zero, the estimated DC-link voltage is equal to the measured DC-link voltage.

$$\hat{v}_{dc}(t) \approx v_{dc}(t) \quad (11)$$

When the estimated DC-link voltage is substituted for the measured DC-link voltage, under steady state conditions, the estimated q-axis current is approximately the reference of q-axis current.

Thus, a new PI controller is developed to obtain the estimated DC-link voltage using the difference between the reference and measured q-axis currents. The proposed PI controller is shown in Fig. 8.

When a fault is diagnosed, the estimated value can be substituted for the measured value (the wrong value) at the same time for implementing fault-tolerant control in the inverter system. The flowchart for the fault diagnosis and fault-tolerant control is given in Fig. 9. The proposed PI controller is reflected in Fig. 10.

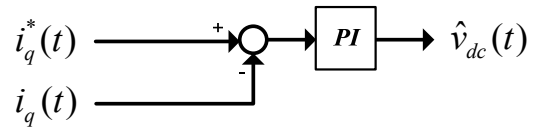


Fig. 8. The proposed PI controller of DC-link voltage estimation

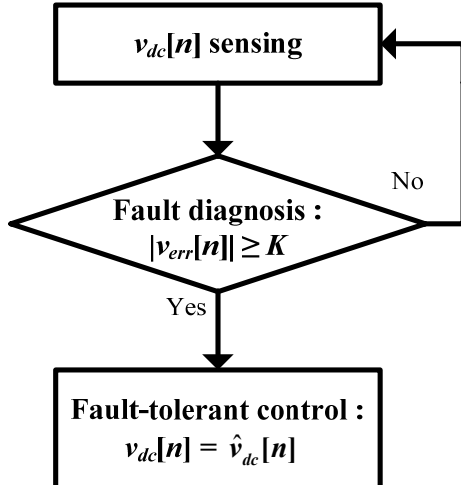


Fig. 9. The flowchart for fault diagnosis and fault-tolerant control

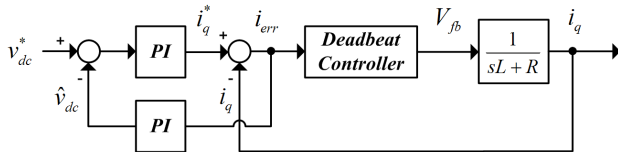


Fig. 10. The modified DC-link voltage and current controller

4. The simulation results

The proposed algorithm was verified by performing a simulation with PSIM software. The parameters used in the simulation are listed in Table 1.

The simulation responses of the fault diagnosis of the DC-link voltage sensor are shown in Fig. 11. At $t = 1.2$ s, because of the fault in the DC-link sensor, the measured voltage is less than the estimated voltage.

The error rate is calculated as $v_{err} = (550 - 600) / 600 = -$

Table 1. The parameters of the simulation

Parameter	Value
Grid phase voltage	E_{max}
Grid frequency	f
Grid-side inductor	L
Grid-side resistor	R
Error range	K
Sampling period	T_s
DC-link capacitor	C_{dc}
DC-link reference voltage	v_{dc}^*

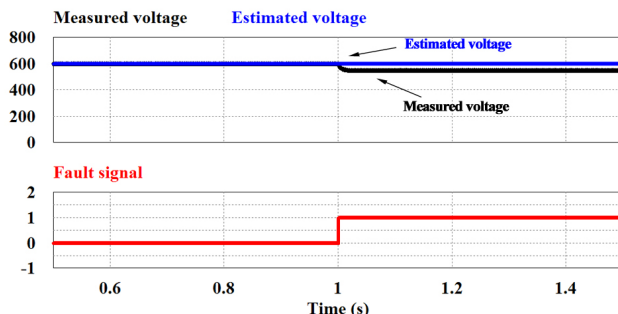


Fig. 11. Fault diagnosis of the DC-link voltage sensor

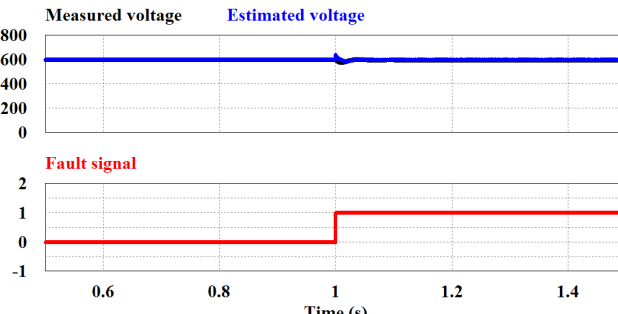


Fig. 12. Fault-tolerant control of the DC-link voltage sensor

0.083 by using Eq. (7). Because the error rate is greater than the error range, the fault is detected and then the fault signal is changed from 0 to 1.

The simulation responses of the simulation of the fault-tolerant control of the DC-link voltage sensor are shown in Fig. 12. At $t = 1.2$ s, after the fault is detected, the estimated voltage can be substituted for the measured voltage for implementing fault-tolerant control. The fault-tolerant controlled DC-link voltage shows the correct value within a settling time of approximately 5 ms.

The simulation responses of the estimated voltage value resulting from the change in the DC-link voltage are shown in Fig. 13. At $t = 2.5$ s, to see how well the estimated voltage can follow the measured voltage, the reference voltage was changed from 600 V to 700 V. The estimated voltage follows the measured voltage within a settling time of approximately 40 ms.

To implement MPPT control, the solar cell must be represented by a simple equivalent model. The I-V (dash curve) and P-V (solid curve) characteristics plots obtained using MATLAB software are shown in Fig. 14. From the P-V curve, it can be seen that the optimal operating voltage is 445 V at the maximum power point ($P = 3991 W$). From the I-V curve, it can be seen that the optimal operating current is 8.968 A at a voltage of $V = 445 V$.

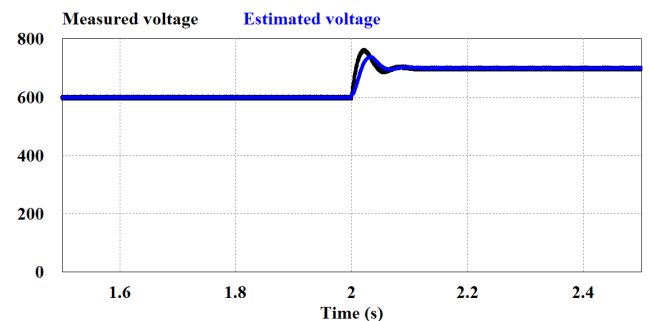


Fig. 13. The estimated value resulting from the DC-link voltage change

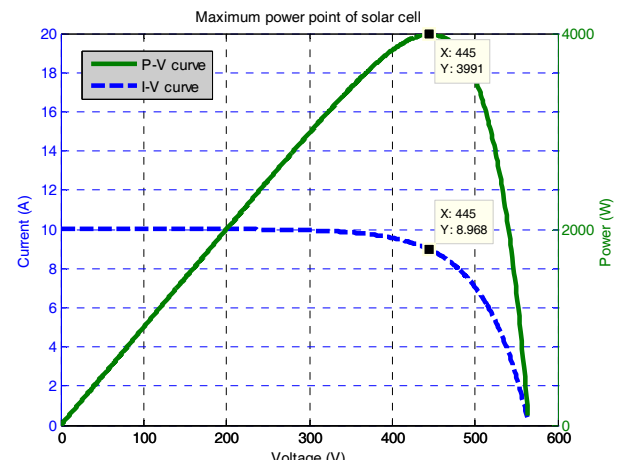


Fig. 14. The maximum power point of the solar cell

The values of power, current, and voltage obtained from the simulation results are shown in Fig. 15. The power (3983 W), current (8.952 A), and voltage (445 V) correspond to the modeled values shown in Fig. 14. According to these results, MPPT control works well under the fault-tolerant control.

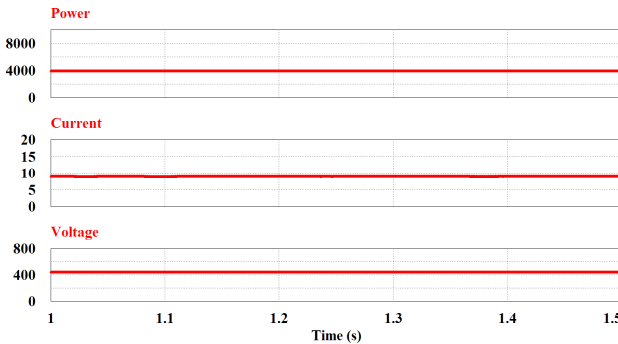


Fig. 15. MPPT control under the fault-tolerant control

5. The experimental results

The overall system of the 4kW PV PCS with grid connection, as shown in Fig. 16, is implemented fully in the software by adopting a 32-bit DSP TMS320F28335.

The experimental responses of the fault diagnosis of the

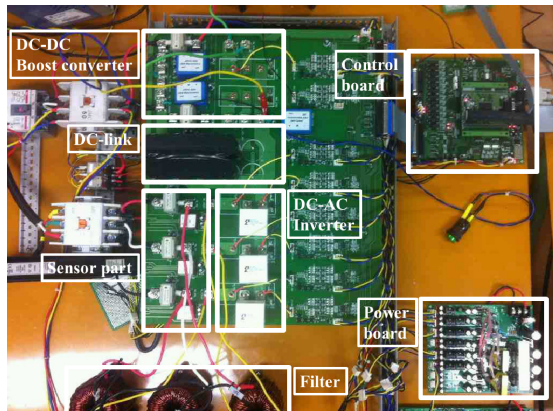


Fig. 16. The prototype of 4kW PV PCS

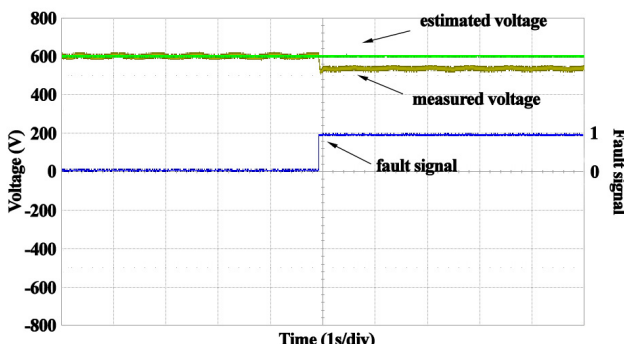


Fig. 17. Fault diagnosis of the DC-link voltage sensor

DC-link voltage sensor are shown in Fig. 17. When a fault occurs, the fault signal is changed from 0 to 1. The experimental results shown in Fig. 17 match the simulation results shown in Fig. 11.

The experimental responses of the fault-tolerant control of the DC-link voltage sensor are shown in Fig. 18. After the fault is diagnosed, the measured voltage is corrected by substituting it with the estimated voltage.

The experimental responses of the estimated value for a DC-link voltage change are shown in Fig. 19. When the reference voltage was changed from 600 V to 700 V, the estimated voltage followed the measured voltage.

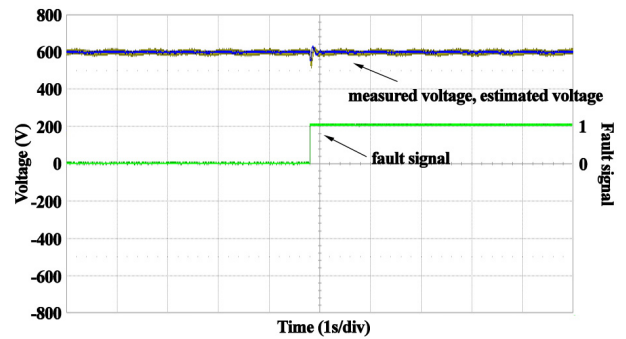


Fig. 18. Fault-tolerant control of the DC-link voltage sensor

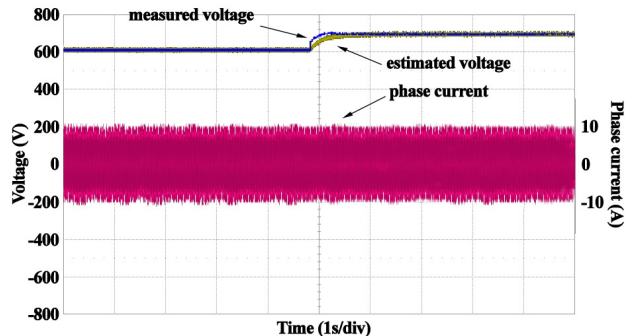


Fig. 19. The estimated value resulting from the DC-link voltage change



Fig. 20. The PV simulator

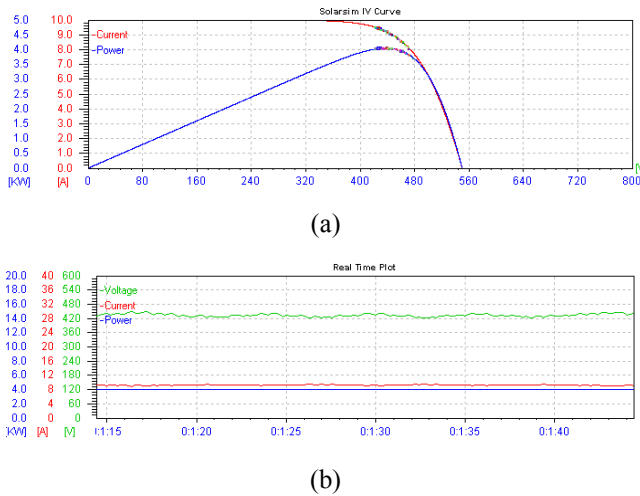


Fig. 21. MPPT control under the fault-tolerant control: (a) The I-V and P-V curves, and (b) the values of V, I, and P at the MPP

Fig. 20 shows the PV simulator for PV PCS. The PV simulator is used in the experiment instead of a PV panel in order to control the input of the PV inverters.

The experimental responses of MPPT control under the fault-tolerant control are shown in Fig. 21. The MPP is located at $V = 445$ V, as shown in Fig. 21(a). The values of power (4 kW), current (8.95 A), and voltage (445 V) shown in Fig. 21(b) correspond to those shown in Fig. 15. Fig. 21 shows that the MPPT control works well.

6. Conclusion

This paper proposes fault diagnosis and fault-tolerant control of a DC-link voltage sensor for grid-connected PV inverters. The P&O algorithm is validated by the simulation and experimental results. By using the DC-link voltage sensorless algorithm, the fault is detected by comparing the measured and estimated voltages. When a fault is detected, the estimated value can be substituted for the measured value at the same time for implementing fault-tolerant control. Under fault-tolerant control, MPPT control works well. Simulation and experimental results are presented to show the effectiveness of the proposed strategy.

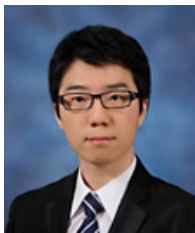
Acknowledgements

This work has been supported by KESRI (Korea Electrical Engineering and Science Research Institute) (2009T100100651), which is funded by MKE (Ministry of Knowledge Economy).

References

- [1] R. J. Wai, W. H. Wang and C. Y. Lin, "High-performance stand-alone photovoltaic generation system," *IEEE Trans. Ind. Electron.*, Vol. 55, No. 1, pp. 240-250, Jan. 2008.
- [2] F. Blaabjerg, R. Teodorescu, M. Liserre and A. Timbus, "Overview of control and grid synchronization for distributed power generation systems," *IEEE Trans. Ind. Electron.*, Vol. 53, No. 5, pp. 1398-1409, Oct. 2006.
- [3] J. Carrasco, L. Franquelo, J. Bialekiewicz, E. Galvan, R. Portillo Guisado, M. Prats, J. Leon and N. Moreno-Alfonso, "Power-electronic systems for the grid integration of renewable energy sources: A survey," *IEEE Trans. Ind. Electron.*, Vol. 53, No. 4, pp. 1002-1016, Jun. 2006.
- [4] S. B. Lee, K. B. Lee, D. C. Lee and J. M. Kim, "An Improved Control Method for a DFIG in a Wind Turbine under an Unbalanced Grid Voltage Condition," *Journal of Electrical Engineering & Technology*, Vol. 5, No. 4, pp. 614-622, Dec. 2010.
- [5] T. F. Wu, C. H. Chang, L. C. Lin and C. L. Kuo, "Power Loss Comparison of Single- and Two-Stage Grid-Connected Photovoltaic Systems," *IEEE Trans. Energy Convers.*, Vol. 26, No. 2, pp. 707-715, Jun. 2011.
- [6] H. S. Bae, J. H. Park, B. H. Cho, and G. J. Yu, "New MPPT Control Strategy for Two-Stage Grid-Connected Photovoltaic Power Conditioning System," *Journal of Power Electronics*, Vol. 7, No. 2, pp. 174-180, Apr. 2007.
- [7] Y. J. Ko and K. B. Lee, "Fault Diagnosis of a Voltage-Fed PWM Inverter for a Three-Parallel Power Conversion System in a Wind Turbine," *Journal of Power Electronics*, Vol. 10, No. 6, pp. 686-693, Nov. 2010.
- [8] U. M. Choi, H. G. Jeong, K. B. Lee, and F. Blaabjerg, "Method for Detecting an Open-Switch Fault in a Grid-Connected NPC Inverter System," *IEEE Trans. Power Electron.*, Vol. 27, No. 6, pp. 2726-2739, Jun. 2012.
- [9] J. M. Kwon, B. H. Kwon and K. H. Nam, "Three-phase photovoltaic system with three-level boosting MPPT control," *IEEE Trans. Power Electron.*, Vol. 23, No. 5, pp. 2319-2327, Sep. 2008.
- [10] Q. Zeng and L. Chang, "An advanced SVPWM-based predictive current controller for three-phase inverters in distributed generation systems," *IEEE Trans. Ind. Electron.*, Vol. 55, No. 3, pp. 1235-1246, Mar. 2008.
- [11] S. Saggini, W. Stefanutti, E. Tedeschi and P. Mattavelli, "Digital deadbeat control tuning for dc-dc converters using error correlation," *IEEE Trans. Power Electron.*, Vol. 22, No. 4, pp. 1566-1570, Jul. 2007.
- [12] H. G. Jeong, H. S. Roh, and K. B. Lee, "An Improved Maximum Power Point Tracking Method for Wind

- Power Systems," *Energies*, Vol. 5, No. 5, pp. 1339-1354, May 2012.
- [13] Z. Wang and L. Chang, "A DC voltage monitoring and control method for three-phase grid-connected wind turbine inverters," *IEEE Trans. Power Electron.*, Vol. 23, No. 3, pp. 1118-1125, May. 2008.
- [14] Z. Wang, L. Chang and M. Mao, "Dc voltage sensorless control method for three-phase grid-connected inverters," *IET Power Electron.*, Vol. 3, iss. 4, pp. 552-558, July. 2010.



Gwang-Seob Kim He received the B.S. degree in Electrical and Computer Engineering from Ajou University, Suwon, Korea, in 2011. He is currently working toward the M.S. degree at Ajou University, Suwon, Korea. His research interests are renewable energy conversion and battery charging system.



Kyo-Beum Lee He received the B.S. and M.S. degrees in Electrical and Electronic Engineering from the Ajou University, Korea, in 1997 and 1999, respectively. He received the Ph.D. degree in electrical engineering from the Korea University, Korea in 2003. From 2003 to 2006, he was with the Institute of Energy Technology, Aalborg University, Aalborg, Denmark. From 2006 to 2007, he was with the Division of Electronics and Information Engineering, Chonbuk National University, Jeonju, Korea. In 2007 he joined the Division of Electrical and Computer Engineering, Ajou University, Suwon, Korea. He is an associate editor of the IEEE Transactions on Power Electronics, Industrial Electronics, and the Journal of Power Electronics. His research interests include electric machine drives, renewable power generations, and electric vehicles.



Dong-Choon Lee He received his B.S., M.S., and Ph.D. in Electrical Engineering from Seoul National University, Seoul, Korea, in 1985, 1987, and 1993, respectively. He was a Research Engineer with Daewoo Heavy Industry from 1987 to 1988. Since 1994, he has been a faculty member in the Department of Electrical Engineering, Yeungnam University, Gyeongbuk, Korea. He is serving as a Publication Editor, Journal of Power Electronics, the Korean Institute of Power Electronics, Korea. As a Visiting Scholar, he joined the Power Quality Laboratory, Texas A&M University in 1998, the Electrical Drive Center, University of Nottingham, U.K. in 2001, the Wisconsin Electric Machines & Power Electronic Consortium, University of Wisconsin, Madison in 2004, and the FREEDM System Center, North Carolina State University, in 2011 and 2012, in U.S.A. His research interests include ac machine drives, control of power converters, wind power generation, and power quality.



Jang-Mok Kim He received his B.S. from Pusan National University in 1988, and his M.S. and Ph.D. from Seoul National University, Korea, in 1991 and 1996, respectively, in the department of Electrical Engineering. From 1997 to 2000, he was a Senior Research Engineer with the Korea Electrical Power Research Institute (KEPRI). Since 2001, he has been with the School of Electrical Engineering, Pusan National University (PNU), where he is currently a Faculty Member. In addition, he is a Research Member of the Research Institute of Computer Information and Communication at PNU, and the head of LG smart control center. His present interests include the control of electric machines, electric vehicle propulsion, and power quality.